Computation of Weakly Ionized Hypersonic Flows in Thermochemical Nonequilibrium

Graham V. Candler*
North Carolina State University, Raleigh, North Carolina 27695
and
Robert W. MacCormack†
Stanford University, Stanford, California 94305

A numerical method to compute a two-dimensional hypersonic flowfield that is weakly ionized and in thermochemical nonequilibrium has been developed. Such a flowfield is described by coupled partial differential equations for the conservation of species mass, mass-averaged momentum, vibrational energy of each diatomic species, electron energy, and total energy. The steady-state solution to these fully coupled equations has been obtained for a gas composed of seven chemical species and characterized by six temperatures using an implicit Gauss-Seidel line relaxation technique. The computed electron number densities in the flowfield of a sphere cone compare well with experimental results.

Nomenclature

c_s = mass fraction of species s, $= \rho_s/\rho$
c_{vs} = translational-rotational specific heat
$\mathcal{D}_s$ = diffusion coefficient of species s
E = total energy per unit volume
E_e, e_e = electron energy per unit volume, mass
E_{vs}, e_{vs} = vibrational energy per unit volume, mass
$\bar{E}_i$ = electric field
e = electron charge
e^*_{vs} = equilibrium vibrational energy per unit mass
F, G = inviscid fluxes in x and y directions
F_v, G_v = viscous fluxes in x and y directions
h_s = enthalpy per unit mass of species s
h^o_s = heat of formation of species s
K_{eql} = equilibrium constant for reaction l
k_{flm}, k_{blm} = reaction rates for reaction l, partner m
k_{vs} = conductivity of e_{vs}
$\mathcal{L}e$ = Lewis number, $= \rho c_p \mathcal{D}/\kappa$
$\mathcal{M}$ = Mach number
M_s = atomic mass of species s
N_s = number density of species s
$\hat{N}$ = Avogadro number
P_{sr} = probability of a r to s $v - v$ exchange
p_s = pressure of species s
Q_{e-vs} = electron-vibration energy transfer rate
Q_{T-e} = translation-electron energy transfer rate
Q_{T-vs} = translation-vibration energy transfer rate
Q_{v-vs} = vibration-vibration energy transfer rate
q_{ej} = electron heat flux
q_j = translational-rotational heat flux
q_{vsj} = vibrational heat flux of species s
R = universal gas constant
Re = Reynolds number based on nose radius
r_n = nose radius
T = translational-rotational temperature
T_e = electron temperature
T_{vs} = vibrational temperature of species s
t = time
U = vector of conserved quantities
u_i = i direction velocity
v_{si} = i direction diffusion velocity of species s
w_s = chemical source term for species s
Z_s = charge number of species s
Z_{sr} = $s - r$ collision number per unit volume
θ_m = characteristic temperature of reaction m
θ_{vs} = characteristic temperature of vibration
μ = mass-averaged viscosity coefficient
κ = conductivity of T
ρ = density, $= \Sigma_s \rho_s$
ρ_s = density of species s
σ_{sr} = collision cross section
τ_{es} = electron-vibration relaxation time
τ_{ij} = mass-averaged shear stress tensor
τ_{sr} = Landau-Teller relaxation time

Presented as Paper 88-0511 at the AIAA 26th Aerospace Sciences Meeting, Reno, NV, Jan. 11–14, 1988; received March 1, 1990; revision received Aug. 14, 1990; accepted for publication Aug. 31, 1990.

*Assistant Professor, Department of Mechanical and Aerospace Engineering, Campus Box 7910. Member AIAA.
†Professor, Department of Aeronautics and Astronautics. Member AIAA.

Introduction

SEVERAL conceptual designs for vehicles that would fly in the atmosphere at hypersonic speeds have been developed recently.[1] For typical flight conditions, the air that envelops these vehicles is chemically reacted, vibrationally excited, and ionized. These reaction and excitation processes occur at rates similar to the rate of fluid motion, which results in a state of thermochemical nonequilibrium. The thermochemical state of the gas influences its dynamics and affects the aerodynamic forces and heat transfer acting on the vehicle.

The flowfield around a hypersonic vehicle is described by the Navier-Stokes equations that have been augmented to include a conservation equation for the mass of each chemical species and for each vibrational energy. For cases where ionization is important, a conservation equation for electron energy is also required. In the past, there have been two standard approaches to solving this equation set. One approach is to uncouple the chemical and thermal rate equations from the fluid equations and solve the two equation sets separately.[2] The chemistry influences the fluid variables after each iteration or series of iterations. This method has the advantage that it is relatively easy to implement and may be used with an existing Navier-Stokes algorithm, but problems with achieving convergence have been encountered. The second method involves solving the entire equation set simultaneously. The advantage of using this technique is that the nonequilibrium effects influence the flowfield directly.[3-8]

In this paper, the fully coupled equation set is solved using a numerical method based on the implicit Gauss-Seidel line relaxation technique discussed by MacCormack.[8–10] The flux vectors are differenced using flux-vector splitting to maintain numerical stability. The entire equation set, including the chemical and thermal source terms, is treated implicitly so that the large source terms do not appreciably degrade the rate of convergence to a steady-state solution. Results have been obtained for a gas made up of seven chemical species (N_2, O_2, NO, NO^+, N, O, and e^-) and characterized by six temperatures, which are one translational-rotational temperature, four vibrational temperatures (one vibrational temperature per diatomic species), and an electron temperature.

Governing Equations

The equations that describe the weakly ionized, thermochemical nonequilibrium flow over a hypersonic vehicle have been developed by Lee.[11] With a multicomponent gas that is characterized by a translational-rotational temperature, separate vibrational temperatures for each diatomic species, and an electron translational temperature, we must solve the following equations.

One mass conservation equation for each species,

$$\frac{\partial \rho_s}{\partial t} + \frac{\partial}{\partial x_j}(\rho_s u_j) = -\frac{\partial}{\partial x_j}(\rho_s v_{sj}) + w_s \tag{1}$$

A mass-averaged momentum equation,

$$\frac{\partial}{\partial t}(\rho u_i) + \frac{\partial}{\partial x_j}(\rho u_i u_j + p\delta_{ij}) = -\frac{\partial \tau_{ij}}{\partial x_j} + \sum_s eN_s Z_s \tilde{E}_i \tag{2}$$

A vibrational energy equation for each diatomic species,

$$\frac{\partial E_{vs}}{\partial t} + \frac{\partial}{\partial x_j}(E_{vs}u_j) = -\frac{\partial}{\partial x_j}(E_{vs}v_{sj}) - \frac{\partial q_{vsj}}{\partial x_j} + Q_{T-vs} + Q_{v-vs} + Q_{e-vs} + w_s e_{vs} \tag{3}$$

An electron energy equation,

$$\frac{\partial E_e}{\partial t} + \frac{\partial}{\partial x_j}[(E_e + p_e)u_j] = -\frac{\partial}{\partial x_j}[(E_e + p_e)v_{ej}] - \frac{\partial q_{ej}}{\partial x_j} - \frac{\partial}{\partial x_j}[(u_i + v_{ei})\tau_{eij}] - N_e e\tilde{E}_i(u_i + v_{ei}) + Q_{T-e} - \sum_s Q_{e-vs} + w_e e_e \tag{4}$$

A total energy equation

$$\frac{\partial E}{\partial t} + \frac{\partial}{\partial x_j}[(E + p)u_j] = -\frac{\partial}{\partial x_j}(q_j + q_{vj} + q_{ej}) - \frac{\partial}{\partial x_j}(u_i\tau_{ij}) - \frac{\partial}{\partial x_j}\sum_s v_{sj}\rho_s h_s + \sum_s eN_s Z_s \tilde{E}_i u_{si} \tag{5}$$

Equations of State

The caloric equation of state for the mass-averaged gas is derived by subtracting the vibrational, kinetic, electron, and chemical energies from the total energy to yield the energy in the translational and rotational modes. Assuming that the rotational energy modes are in equilibrium with the translational modes, we can determine the translational-rotational temperature T,

$$\sum_{s\neq e} \rho_s c_{vs} T = E - \frac{1}{2}\sum_{s\neq e}\rho_s u_i u_i - \sum_s E_{vs} - E_e - \sum_s \rho_s h_s^o \tag{6}$$

The pressure is the sum of the partial pressures,

$$p = \sum_{s\neq e} \rho_s \frac{R}{M_s} T + p_e \tag{7}$$

The equations of state for the electrons are

$$\rho_e c_{ve} T_e = E_e - \frac{1}{2}\rho_e u_i u_i, \qquad p_e = \rho_e \frac{R}{M_e} T_e \tag{8}$$

We have assumed that the energy contained in the excited electronic states of the molecules is negligible relative to the energy contained in the other modes.

Simplifications to the Conservation Equations

We may simplify the equation set by considering the electron momentum equation,

$$\frac{\partial}{\partial t}(\rho_e u_{ei}) + \frac{\partial}{\partial x_j}(\rho_e u_{ei}u_{ej} + p_e\delta_{ij}) = -\frac{\partial \tau_{eij}}{\partial x_j} - eN_e\tilde{E}_i \tag{9}$$

If we take the ratio of the dynamic pressure of the electron gas to the electron pressure and assume that the electron speed and temperature are about the same as the bulk gas, we have

$$\frac{\rho_e u_e^2}{p_e} = \frac{M_e u_e^2}{RT_e} \simeq \frac{M_e u^2}{RT} \simeq \frac{M_e}{M}\mathcal{M}^2 \tag{10}$$

The ratio M_e/M is of the order of 10^{-6} and for conditions of interest, and the square of the Mach number will be of the order of 10^3 at most. Therefore, we can neglect the electron dynamic pressure relative to the electron pressure. The electron shear stress is also small relative to the electron pressure, and because we are solving for a steady-state, we may neglect the time derivative of the momentum. Therefore, the electric field may be expressed as

$$\tilde{E}_i \simeq -\frac{1}{N_e e}\frac{\partial p_e}{\partial x_i} \tag{11}$$

This expression is used in the mass-averaged momentum and total energy equations.

Shear Stress Tensor and Heat Conduction

The shear stress tensor and heat conduction vectors are given by

$$\tau_{ij} = -\mu\left(\frac{\partial u_i}{\partial x_j} + \frac{\partial u_j}{\partial x_i}\right) + \frac{2}{3}\mu\frac{\partial u_k}{\partial x_k}\delta_{ij} \tag{12}$$

$$q_j = -\kappa\frac{\partial T}{\partial x_j}, \qquad q_{vsj} = -k_{vs}\frac{\partial e_{vs}}{\partial x_j}, \qquad q_{ej} = 0 \tag{13}$$

The conduction of vibrational energy is treated in this fashion because of the nonlinear variation of vibrational temperature with energy.[12] The conduction of electron energy has been neglected. A model for the reacting gas viscosity developed by Blottner et al.[13] is used to determine the species viscosity. The conductivity of the translational-rotational temperature and vibrational energy for each species are given by

$$\kappa_s = \mu_s\left(\frac{5}{2}c_{v\text{trans}} + c_{v\text{rots}}\right), \qquad k_{vs} = c_s\mu_s \tag{14}$$

which are derived from an Eucken relation.[12] The total viscosity and conductivity of the gas are then calculated using Wilke's semiempirical mixing rule.[14]

Diffusive Fluxes

For simplicity, the diffusion velocities of each component of the gas mixture are assumed to be proportional to the gradients of the mass fractions

$$\rho_s v_{sj} = -\rho \mathcal{D}_s \frac{\partial c_s}{\partial x_j} \tag{15}$$

The expression for the species diffusion coefficients is obtained by assuming a constant Lewis number ($\mathcal{L}_e = 1.4$). The diffusion coefficients for ions and electrons are assumed to be doubled (i.e., the ambipolar diffusion assumption holds). A more exact formulation would involve the inclusion of multicomponent diffusion terms, as discussed by Blottner et al.[13]

Energy Exchange Mechanisms

The energy exchange mechanisms that appear on the right side of Eqs. (3) and (4) must be modeled. The models that have been published previously are outlined, and a model for vibration-vibration energy exchanges is briefly derived later.

Translation-Vibration Energy Exchanges

The rates of energy exchange between the translational and vibrational energy modes Q_{T-vs} are assumed to be of the Landau-Teller form,

$$Q_{T-vs} = \rho_s \frac{e_{vs}^*(T) - e_{vs}}{\langle \tau_s \rangle} \tag{16}$$

The Landau-Teller relaxation time is given by an expression from Lee,[11]

$$\langle \tau_s \rangle = \frac{\Sigma_r N_r}{\Sigma_r N_r / \tau_{sr}}, \qquad \text{for } r \neq e \tag{17}$$

An expression developed by Millikan and White[15] yields the relaxation time τ_{sr}.

Translation-Electron Energy Exchanges

The energy transfer rate between the heavy-particle and electron translational modes Q_{T-e} is given by an expression derived from Lee[11]

$$Q_{T-e} = 3R\rho_e(T - T_e)\sqrt{\frac{8RT_e}{\pi M_e}} \sum_{r \neq e} \frac{\rho_r \hat{N}}{M_r^2} \sigma_{er} \tag{18}$$

where σ_{er}, $r \neq$ ions, are the collision cross sections for electron-neutral interactions. The functional form of these parameters is not well known, and for this work, a constant $\sigma_{er} = 10^{-20}$ m^2 was assumed. For the case of electron-ion interactions, the effective Coulomb cross section is given by[11]

$$\sigma_{e,\text{ions}} = \frac{8\pi}{27} \frac{e^4}{k^2 T_e^2} \ln\left[1 + \frac{9k^3 T_e^3}{4\pi N_e e^6}\right] \tag{19}$$

Electron-Vibration Energy Exchanges

The coupling of the electron energy with the vibrational energy of diatomic nitrogen is strong, but between the other molecules it is negligibly weak.[16] The rate of energy transfer between electron translational modes and nitrogen vibrational modes Q_{e-vs} is assumed to be of Landau-Teller form,[12]

$$Q_{e-vs} = \rho_s \frac{M_s}{M_e} \frac{e_{vs}^*(T_e) - e_{vs}}{\tau_{es}}, \qquad \text{for } s = \mathrm{N_2} \tag{20}$$

where the relaxation time τ_{es} is a function of electron temperature and pressure derived by Lee.[16]

Vibration-Vibration Energy Exchanges

The current formulation allows different vibrational temperatures; however, as one species becomes excited, it tends to transfer its vibrational energy to the other species in vibration-vibration ($v - v$) energy exchanges. The rate of vibrational energy transfer from species r to s is the product of the probability of a $v - v$ exchange, the number of collisions, and the change in the energy during the collision. This may be written as

$$Q_{v-vsr} = P_{sr} \cdot Z_{sr} \cdot \Delta\varepsilon_{vsr} \tag{21}$$

where $\Delta\varepsilon_{vsr}$ is the change in the s particle vibrational energy due to the $v-v$ energy transfer. Assume that after the collision, the two collision partners have the same vibrational temperature T'_{vsr}. Thus, balancing the energy before and after the collision yields

$$\varepsilon_{vs}(T_v) + \varepsilon_{vr}(T_v) = \varepsilon_{vs}(T'_{vsr}) + \varepsilon_{vr}(T'_{vsr}) \tag{22}$$

From this expression, we can solve for T'_{vsr} using the definition of the vibrational energy per particle for a simple harmonic oscillator

$$\varepsilon_{vs}(T_v) = \frac{R}{\hat{N}} \frac{\theta_{vs}}{e^{\theta_{vs}/T_v} - 1} = \frac{M_s}{\hat{N}} e_{vs}(T_v) \tag{23}$$

Thus, the change in the s particle vibrational energy due to a collision with r is

$$\Delta\varepsilon_{vsr} = \varepsilon_{vs}(T'_{vsr}) - \varepsilon_{vs} \tag{24}$$

And, therefore, for n species, the $v - v$ energy transfer rate is

$$Q_{v-vs} = \sum_{r \neq s}^{n} Q_{v-vsr} = \sum_{r \neq s}^{n} P_{sr} \cdot Z_{sr} \cdot \frac{M_s}{\hat{N}} [e_{vs}(T'_{vsr}) - e_{vs}] \tag{25}$$

Z_{sr} is determined from kinetic theory,[12] and the probabilities of an exchange have been measured for several molecules.[17] For temperatures of interest (above 2000 K), P_{sr} is typically of the order of 0.01, and for this work, it has been assumed to be constant at that value.

Chemical Source Terms

The chemical source terms are derived from the reactions that occur between the components of the gas. The primary chemical reactions between the seven species considered in this work are

$$\mathrm{N_2} + M \rightleftharpoons 2\mathrm{N} + M \tag{26a}$$

$$\mathrm{O_2} + M \rightleftharpoons 2\mathrm{O} + M \tag{26b}$$

$$\mathrm{NO} + M \rightleftharpoons \mathrm{N} + \mathrm{O} + M \tag{26c}$$

$$\mathrm{N_2} + \mathrm{O} \rightleftharpoons \mathrm{NO} + \mathrm{N} \tag{26d}$$

$$\mathrm{NO} + \mathrm{O} \rightleftharpoons \mathrm{O_2} + \mathrm{N} \tag{26e}$$

$$\mathrm{N} + \mathrm{O} \rightleftharpoons \mathrm{NO^+} + e^- \tag{26f}$$

where M represents any species. From these reactions, the source terms w_s may be constructed from the Law of Mass Action.[12] These source terms are governed by forward and backward reaction rates that have the form

$$k_{fl}(\bar{T}) = C_{fl} \bar{T}^{\eta l} \exp(-\theta_l / \bar{T}) \tag{27a}$$

$$k_{bl}(\bar{T}) = \frac{k_{fl}(\bar{T})}{K_{eql}(\bar{T})} \tag{27b}$$

where the constants C_{fl}, η_l, and θ_l are experimentally determined. As discussed by Park,[3,18,19] the reaction rates will be a function of different temperatures depending on the type of reaction. Consider the first three reactions where the impacting particle M is a heavy species. The forward reaction rate will be a function of the vibrational excitation of the diatomic molecule and the translational temperature of the impacting heavy particle. Thus, using the arguments of Park,[19] we can postulate an average temperature that governs this reaction rate to be

$$k_{flm} = k_{flm}(\bar{T}), \qquad \bar{T} = \sqrt{TT_{vl}}, \qquad \text{for } l = 1,2,3, \quad m \neq e^- \tag{28}$$

The backward reaction rates will depend only on the translational temperatures of the impacting particles,

$$k_{blm} = k_{blm}(T), \qquad \text{for } l = 1,2,3, \quad m \neq e^- \tag{29}$$

For the case where the impacting particle is an electron, the forward rate will depend on the average of the vibrational temperature and the electron translational temperature,

$$k_{flm} = k_{flm}(\bar{T}), \qquad \bar{T} = \sqrt{T_{vl}T_e}, \quad \text{for } l = 1,2,3, \quad m = e^- \tag{30}$$

Similarly, the backward reaction rate is governed by an average temperature

$$k_{blm} = k_{blm}(\bar{T}), \qquad \bar{T} = \sqrt{TT_e}, \qquad \text{for } l = 1,2,3, \quad m = e^- \tag{31}$$

The forward and backward rates of reactions 4 and 5 will depend only on the relative speed of the impacting molecules, which implies that $\bar{T} = T$. The forward rate of reaction 6 will also be governed by the translational temperature of the impacting atoms. However, its backward reaction rate will depend on the vibrational temperature of NO^+ and the translational temperature of the electrons,

$$k_{b6} = k_{b6}(\bar{T}), \qquad \bar{T} = \sqrt{T_{vNO^+}T_e} \tag{32}$$

The forward reaction rates for the first five reactions were taken from Park.[3] The coefficients for the sixth reaction came from Wray.[13,20] The expressions for the equilibrium constants K_{eql} were taken from Park.[3]

Boundary Conditions

The boundary conditions for the problem are as follows. The freestream is supersonic so that all flow variables are known. The outflow is also supersonic, and, therefore, a zero-gradient exit condition is appropriate. The wall boundaries are specified by assuming either an adiabatic or fixed-wall temperature, a no-slip velocity condition, and a zero normal gradient of pressure at the wall. In the results presented below, the wall was assumed to be noncatalytic, which implies that the normal gradient of each species mass fraction is zero at the wall. Finite rate catalytic recombination of the atoms at the surface could be included using the expressions developed by Park.[21] Park also states that the electron-ion recombination reaction is perfectly catalyzed at the wall; this would be a more accurate boundary condition.

Numerical Method

The numerical method used to solve the governing equations is based on an implicit Gauss-Seidel line relaxation technique developed by MacCormack.[8-10,22] The algorithm is fully implicit except for some of the minor (non-thin-layer Navier-Stokes) terms. The chemical and thermal source terms are treated implicitly so that the maximum time step is not diminished appreciably from a nonreacting flowfield. The algorithm has been described for perfect gas cases[9,10,22] and for a five-species reacting flow[8] and, therefore, will only be discussed briefly here.

Let us write Eqs (1–5) in two-dimensional conservation-law form

$$\frac{\partial U}{\partial t} + \frac{\partial F}{\partial x} + \frac{\partial G}{\partial y} = -\frac{\partial F_v}{\partial x} - \frac{\partial G_v}{\partial y} + W \tag{33}$$

The inviscid fluxes are homogeneous in U, that is, $F = (\partial F/\partial U)U$. Therefore, for this extended set describing thermochemical nonequilibrium flow, we can use the flux-splitting techniques developed for perfect gas flows. Once the fluxes have been split, they are upwind differenced using one of two flux-splitting methods. In most of the flowfield, the nondissipative flux-splitting technique proposed by MacCormack and Candler[22] is used. However, near large pressure gradients, the Steger-Warming[23] form is employed. The Steger-Warming technique is more dissipative and maintains stability so that the strong bow shock wave may be captured. With the combination of the two flux-splitting algorithms, a blunt body problem with a strong bow shock may be solved without the introduction of significant numerical dissipation in the boundary layer.

Results

The computed cases simulate the RAM-C II flight test, which was a spherically blunted cone with a 0.1524-m nose radius, 9-deg cone half-angle, and a total length of 1.3 m flown into the atmosphere at approximately satellite speed.[24-26] Electron number densities were measured at four axial locations using microwave reflectometers and in the boundary layer using an electrostatic rake.

Computations were performed to replicate the RAM-C II tests at altitudes of 61, 71, and 81 km. This altitude range approximately spans a region of near thermochemical equilibrium at 61 km to strong nonequilibrium at 81 km. The wall temperature was fixed at 1000 K, which is an approximation to the actual wall temperature, which is unknown. The wall was assumed to be noncatalytic. In each case, the freestream velocity was 7650 m/s. The corresponding Mach numbers and Reynolds numbers based on nose radius and freestream conditions are given in Table 1. In each case, the freestream was composed of 79% N_2 and 21% O_2.

Table 1 Freestream conditions for computed cases

Altitude, km	$\mathcal{M}_\infty$	Re
61	23.9	1.95×10^4
71	25.9	6.28×10^3
81	28.3	1.59×10^3

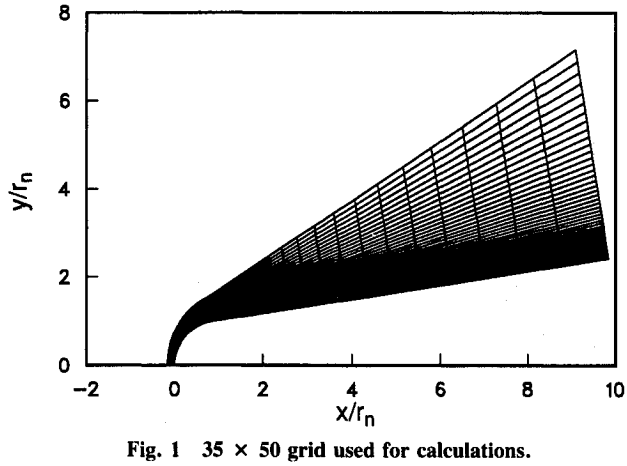

Fig. 1 35 × 50 grid used for calculations.

The computations were performed on body-fitted meshes with 35 points axially along the sphere cone and 50 points in the flowfield normal to the body. Figure 1 shows a mesh used for one of the test cases.

Figures 2–4 compare the computed results with the peak electron number density measured axially along the body at each altitude. These plots show that the electron number density is highest at the nose and falls off rapidly around the shoulder of the body. The fluid carries with it a large number of electrons that have been produced near the nose but have not yet recombined. Thus, although the local temperature is relatively low, the number of electrons remains high in the shoulder region.

Figures 5–7 depict the mass fractions of the major constituents of the gas on the stagnation streamline. These plots are indicative of the degree of chemical nonequilibrium in the flowfield for each case. The dissociation of oxygen molecules

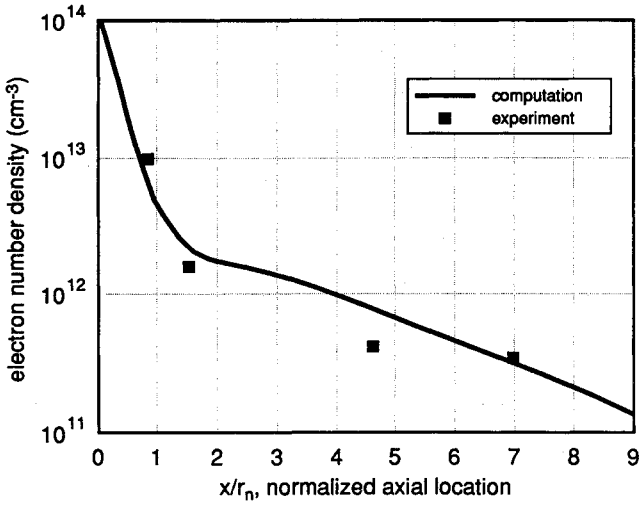

Fig. 2 Comparison of peak electron number density: 61 km; $\mathcal{M}_\infty$ = 23.9; Re = 1.95 × 10⁴.

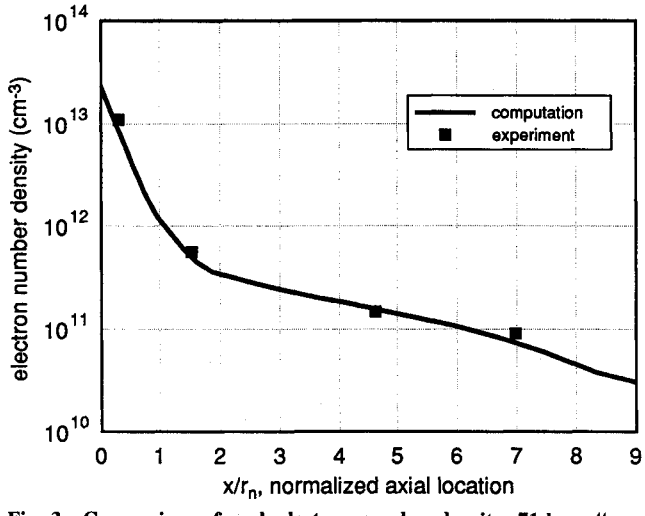

Fig. 3 Comparison of peak electron number density: 71 km; $\mathcal{M}_\infty$ = 25.9; Re = 6.28 × 10³.

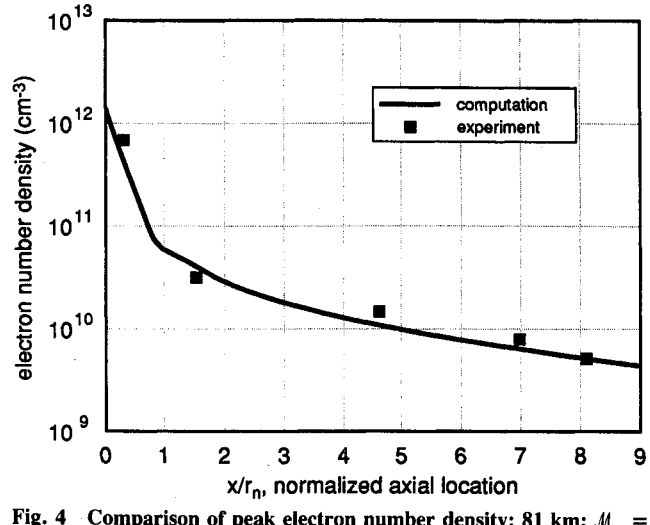

Fig. 4 Comparison of peak electron number density: 81 km; $\mathcal{M}_\infty$ = 28.3; Re = 1.59 × 10³.

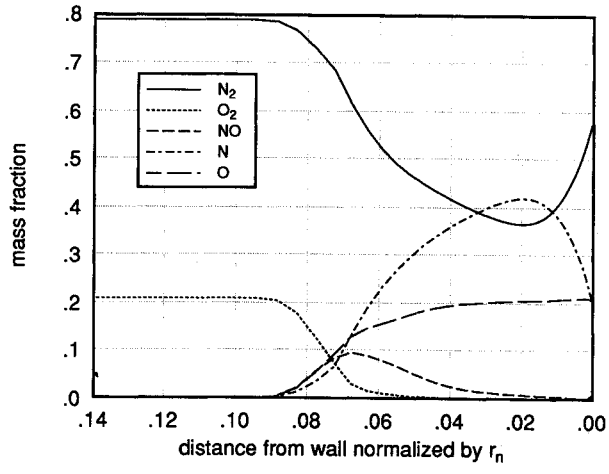

Fig. 5 Mass fractions of the five major species on stagnation streamline: 61 km; $\mathcal{M}_\infty$ = 23.9; Re = 1.95 × 10⁴.

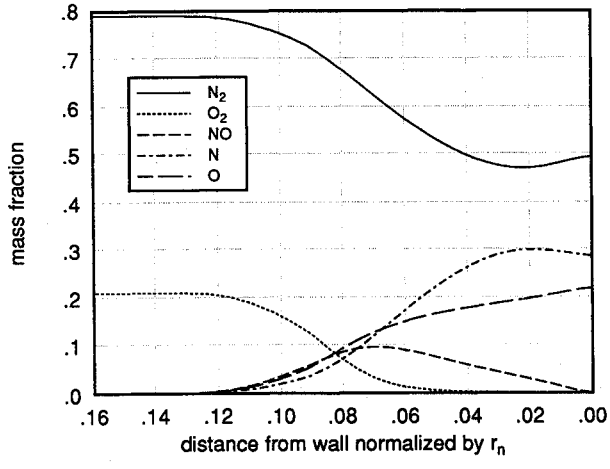

Fig. 6 Mass fractions of the five major species on stagnation streamline: 71 km; $\mathcal{M}_\infty$ = 25.9, Re = 6.28 × 10³.

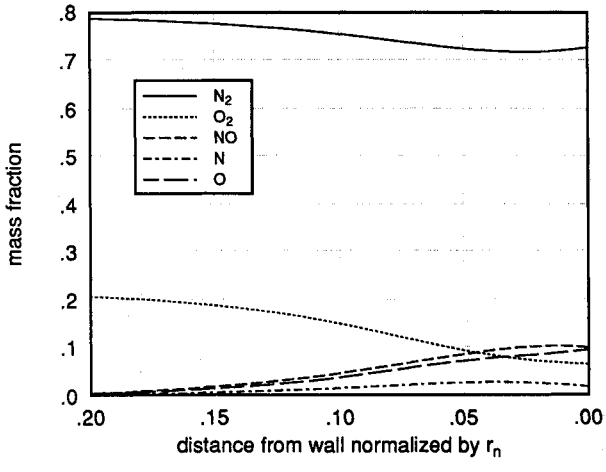

Fig. 7 Mass fractions of the five major species on stagnation streamline: 81 km; $\mathcal{M}_\infty$ = 28.3; Re = 1.59 × 10³.

occurs very rapidly, within about 2% of the nose radius in the 61-km case. At 81 km, the reaction is not complete by the time the gas reaches the wall. Because the density is lower at higher altitudes, there are fewer intermolecular collisions and, thus, the reaction rates are slower. These plots also demonstrate that the bow shock becomes more diffuse at higher altitudes.

Figure 8 is a plot of the mole fractions of the chemical constituents on the stagnation streamline for the 71-km case. The mole fractions of the ions and the electrons are identical on the stagnation streamline and the level of these species is small everywhere. There is no charge separation since the diffusion velocities of the ions and the electrons are identical everywhere. This figure shows the rapidity with which the chemical reactions occur at the shock wave. Figure 8 also demonstrates that the peak mole fraction of electrons occurs in the inviscid region. This indicates that the fully catalytic wall boundary condition for ion-electron recombination suggested by Park[21] would have little effect on the peak electron mole fraction. Thus, although the noncatalytic boundary condition is not accurate, a fully catalytic wall would not significantly change the comparison to the RAM-C experiment.

Three of the six temperatures on the stagnation streamline at 71 km are plotted in Fig. 9. The translational-rotational temperature reaches a peak of about 25,000 K and then decreases toward the wall temperature. The N_2 vibrational temperature moves toward T rapidly and equilibrates with it. The three other vibrational temperatures are very similar on the stagnation streamline and, therefore, were not plotted. This indicates that, with the current vibrational coupling model, the vibrational state of the flowfield may be adequately characterized by one temperature. The vibrational temperatures reach a peak of 11,600 K, which is similar to results presented by Park[19] for approximately the same case. The electron temperature peaks near the wall at about 5300 K. This case is characterized by a large degree of thermal nonequilibrium and, consequently, a one temperature model would be inadequate to describe this flowfield. Figure 9 also shows that the shock wave thickness is a significant portion of the shock standoff distance for the 71-km case. This indicates that the continuum assumption may be suspect and that low density effects such as wall slip and nonlinear stress-strain relations may be important for these conditions.

The remaining figures are contour plots of several different flowfield quantities. Figures 10 and 11 are contours of the translational-rotational temperature and the vibrational temperature of N_2. These two temperatures have the same general distribution, with the peak value at the nose and then a rapid reduction as the gas expands around the shoulder of the body. However, if we examine these figures, we see that the difference in these temperatures has the general trend of $T > T_{vN_2}$ in the nose region and $T < T_{vN_2}$ in the shoulder region. This is typical of a nonequilibrium flowfield where compressions and expansions of the flow change the translational-rotational temperature and the vibrational temperature follows these changes with a finite relaxation time.

Figures 12–14 are contour plots of the species mass fractions of N_2, O_2, and NO^+. They all show the same general features, namely that the gas reacts primarily near the nose and then recombines slowly as it expands and cools in the shoulder region. Figure 13 shows that a large portion of the flowfield is essentially devoid of diatomic oxygen. The final figure is a plot of the ionized species NO^+, which shows that its maximum mass fraction is only 0.08%.

Computer Requirements

The steady-state solutions of the flowfield equations were obtained in approximately 500–700 iterations for the seven-species equation set. The large number of iterations was required in the lower altitude case as the reaction rates are higher and consequently the equations are numerically stiffer than the high altitude case. The CPU time required per time step for a vectorized code was about 1.1 s on a Cray X-MP with the 35 × 50 mesh.

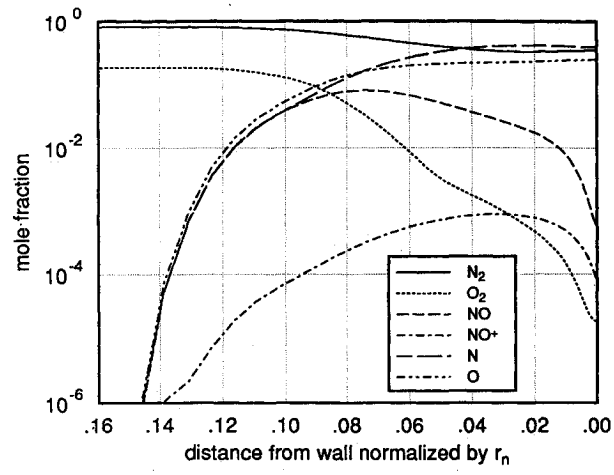

Fig. 8 Mole fractions on stagnation streamline: 71 km; M_∞ = 25.9; Re = 6.28 × 10³.

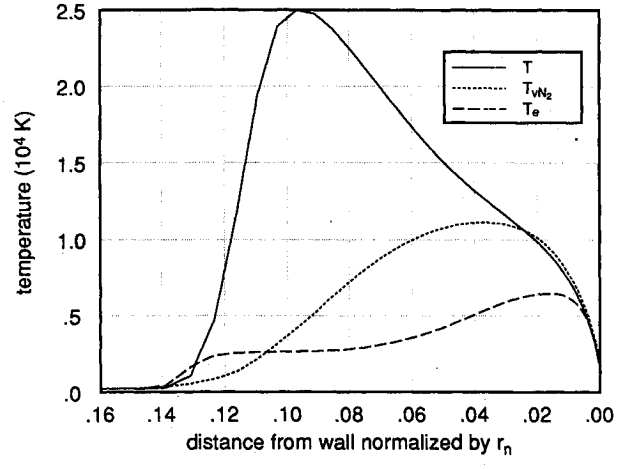

Fig. 9 Temperatures on stagnation streamline: 71 km; M_∞ = 25.9; Re = 6.28 × 10³.

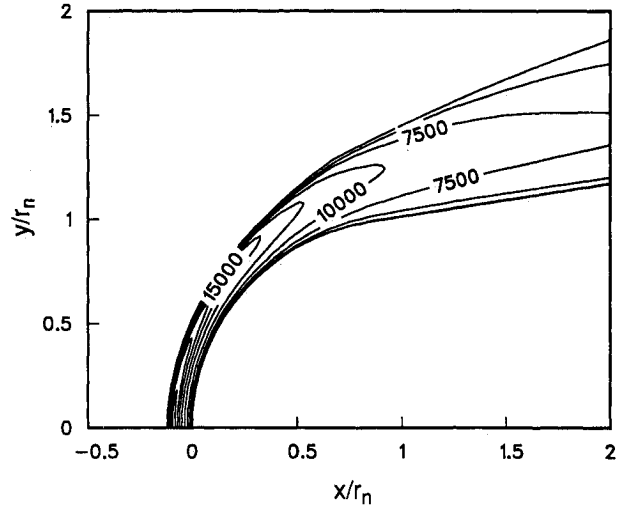

Fig. 10 Contours of translational-rotational temperature (K): 71 km; M_∞ = 25.9; Re = 6.28 × 10³.

Conclusions

A numerical method to solve the fully coupled equations that describe a two-dimensional thermochemical nonequilibrium hypersonic flowfield has been developed. The high temperature, high velocity flow has been represented with a

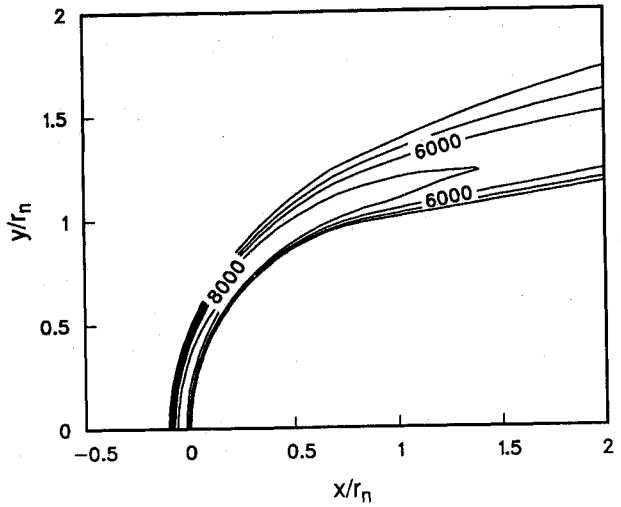

Fig. 11 Contours of N_2 vibrational temperature (K): 71 km; $\mathcal{M}_\infty$ = 25.9; Re = 6.28 × 10^3.

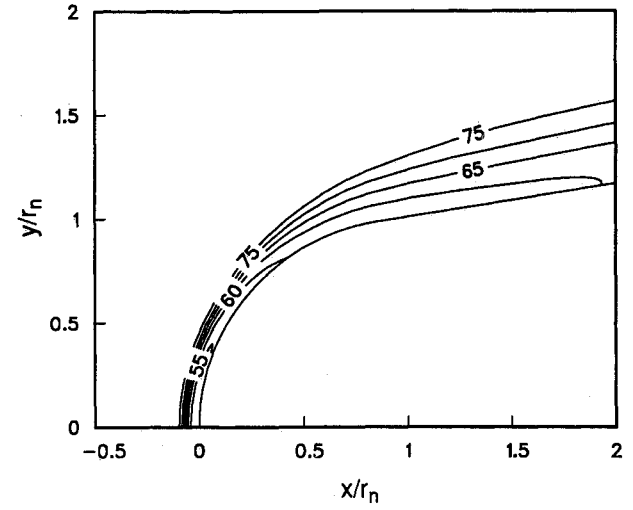

Fig. 12 Contours of N_2 mass fraction (%): 71 km; $\mathcal{M}_\infty$ = 25.9; Re = 6.28 × 10^3.

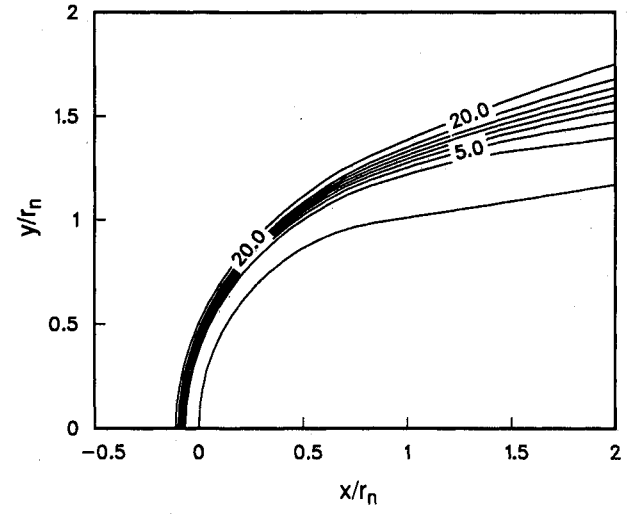

Fig. 13 Contours of O_2 mass fraction (%): 71 km; $\mathcal{M}_\infty$ = 25.9; Re = 6.28 × 10^3.

model that treats the gas as composed of seven chemical constituents and as characterized by one translational-rotational temperature, four vibrational temperatures, and one free electron translational temperature.

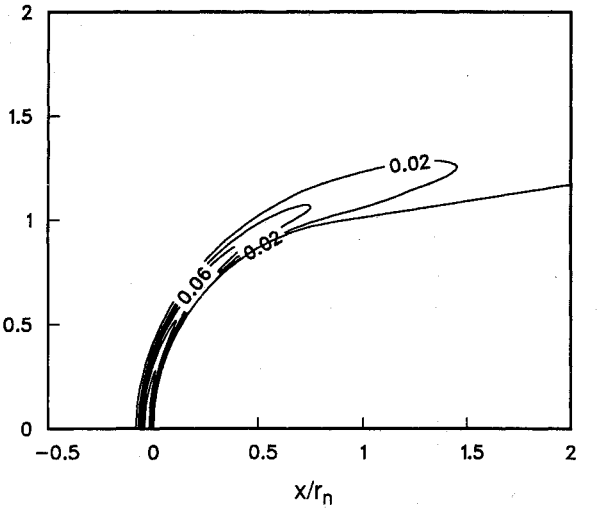

Fig. 14 Contours of NO^+ mass fraction (%): 71 km; $\mathcal{M}_\infty$ = 25.9; Re = 6.28 × 10^3.

The electron number densities computed using the seven-species gas model are in good agreement with the RAM-C II flight experiment. The vibrational state of the flowfield may be approximated with only one vibrational temperature. The use of a multitemperature model is required to correctly describe the thermal state of the gas for these conditions.

The implicit Gauss-Seidel line relaxation method yields results for the fully coupled and numerically stiff equation set in about 600 time steps. Since the description of the flowfield requires a large number of equations, the solution is computationally intensive. However, the numerical method shows promise for the extension of the reacting gas model to include more chemical species, to account for radiation of the flowfield, and to treat the energy exchange mechanisms more accurately.

Acknowledgments

The authors would like to acknowledge the support for this work from SDIO/IST, managed by the Army Research Office, under Contract DAAl03-86-K-0139, the Department of the Air Force under Contract F33615-86-C-3015, and NASA under a Hypersonic Training and Research Grant NAGW 965. The authors would also like to thank Dr. Chul Park of NASA Ames Research Center for his many helpful suggestions.

References

[1]Howe, J. T., "Introductory Aerothermodynamics of Advanced Space Transportation Systems," *Journal of Spacecraft and Rockets*, Vol. 22, No. 1, 1985, pp. 104–111.

[2]Gnoffo, P. A., and McCandless, R. S., "Three Dimensional AOTV Flowfields in Chemical Nonequilibrium," AIAA Paper 86-0230, Jan. 1986.

[3]Park, C., "On Convergence of Computation of Chemically Reacting Flows," AIAA Paper 85-0247, Jan. 1985.

[4]Bussing, T. R. A., and Murman, E. M., "A Finite Volume Method for the Calculation of Compressible Chemically Reacting Flows," AIAA Paper 85-0331, Jan. 1985.

[5]Bussing, T. R. A., "Numerical Investigation of 2-Dimensional H_2-Air Flame Holding Over Ramps and Rearward Facing Steps," AIAA Paper 85-1250, July 1985.

[6]Eberhardt, S., and K. Brown, "A Shock Capturing Technique for Hypersonic, Chemically Relaxing Flows," AIAA Paper 86-0231, Jan. 1986.

[7]Prabhu, D. K., Tannehill, J. C., and Marvin, J. G., "A New PNS Code for Chemical Nonequilibrium Flows," AIAA Paper 87-0284, Jan. 1987.

[8]Candler, G. V., and MacCormack, R. W., "The Computation of Hypersonic Flows in Chemical and Thermal Nonequilibrium," Presented at the Third National Aero-Space Plane Technology Symposium, NASA Ames, Moffett Field, Mountain View CA., June 1987.

[9]MacCormack, R. W., "Current Status of the Numerical Solutions of the Navier-Stokes Equations," AIAA Paper 85-0032, Jan. 1985.
[10]Candler, G. V., and MacCormack, R. W., "Hypersonic Flow Past 3-D Configurations," AIAA Paper 87-0480, Jan. 1987.
[11]Lee, J. H., "Basic Governing Equations for the Flight Regimes of Aeroassisted Orbital Transfer Vehicles," *Progress in Aeronautics and Astronautics: Thermal Design of Aeroassisted Orbital Transfer Vehicles*, Vol. 96, edited by H. F. Nelson, AIAA, New York, 1985, pp. 3–53.
[12]Vincenti, W. G., and Kruger, C. H., Jr., *Introduction to Physical Gas Dynamics*, Krieger, FL, 1965.
[13]Blottner, F. G., Johnson, M., and Ellis, M., "Chemically Reacting Viscous Flow Program for Multi-Component Gas Mixtures," Sandia Laboratories, Albuquerque, NM, Rept. SC-RR-70-754, Dec. 1971.
[14]Wilke, C. R., "A Viscosity Equation for Gas Mixtures," *Journal of Chemical Physics*, Vol. 18, No. 4, 1950, p. 517.
[15]Millikan, R. C., and White, D. R., "Systematics of Vibrational Relaxation," *Journal of Chemical Physics*, Vol. 39, No. 12, 1963, pp. 3209–3213.
[16]Lee, J. H., "Electron-Impact Vibrational Excitation Rates in the Flowfield of Aeroassisted Orbital Transfer Vehicles," *Progress in Aeronautics and Astronautics: Thermophysical Aspects of Re-entry Flows*, Vol. 103, edited by J. N. Moss and C. D. Scott, AIAA, New York, 1986, pp. 197–224.
[17]Taylor, R. L., Camac, M., and Feinberg, R. M., "Measurements of Vibration-Vibration Coupling in Gas Mixtures," *Proceedings of the Eleventh Symposium on Combustion*, The Combustion Institute, Pittsburgh, PA, 1967. Aug. 1966, pp. 49–65.
[18]Park, C., "Assessment of Two-Temperature Kinetic Model for Dissociating and Weakly Ionizing Nitrogen," AIAA Paper 86-1347, June 1986.
[19]Park, C., "Assessment of Two-Temperature Kinetic Model for Ionizing Air," AIAA Paper 87-1574, June 1987.
[20]Bussing, T. R. A., and Eberhardt, S., "Chemistry Associated with Hypersonic Vehicles," AIAA Paper 87-1292, June 1987.
[21]Park, C., *Nonequilibrium Hypersonic Aerodynamics*, Wiley, New York, 1990, pp. 139–142.
[22]MacCormack, R. W., and Candler, G. V., "The Solution of the Navier-Stokes Equations Gauss-Seidel Line Relaxation," *Computers and Fluids*, Vol. 17, No. 1, 1989, pp. 135–150.
[23]Steger, J., and Warming, R. F., "Flux Vector Splitting of the Inviscid Gasdynamics Equations with Application to Finite Difference Methods," NASA TM-78605, 1979.
[24]Akey, N. D., and Cross, A. E., "Radio Blackout Alleviation and Plasma Diagnostic Results from a 25,000 Foot per Second Blunt-Body Reentry," NASA TN D-5615, Feb. 1970.
[25]Grantham, W. L., "Flight Results of 25,000 Foot per Second Reentry Experiment Using Microwave Reflectometers to Measure Plasma Electron Density and Standoff Distance," NASA TN D-6062, Dec. 1970.
[26]Jones, W. L., Jr., and Cross, A. E., "Electrostatic Probe Measurements of Plasma Parameters for Two Reentry Flight Experiments at 25,000 Feet per Second," NASA TN D-6617, Feb. 1972.